SHORT COMMUNICATION

X-ray phase contrast tomography; proof of principle for post-mortem imaging

[1]ANNA ZAMIR, BSc, [2,3]OWEN J ARTHURS, FRCR, PhD, [1]CHARLOTTE K HAGEN, PhD, [1]PAUL C DIEMOZ, PhD, [4]THIERRY BROCHARD, [4]ALBERTO BRAVIN, PhD, [2,3]NEIL J SEBIRE, FRCPATH and [1]ALESSANDRO OLIVO, PhD

[1]Department of Medical Physics and Biomedical Engineering, University College London, London, UK
[2]Great Ormond Street Hospital for Children NHS Foundation Trust, London UK.
[3]Institute of Child Health, University College London, London, UK
[4]European Synchrotron Radiation Facility, Grenoble, France

Address correspondence to: Miss Anna Zamir
E-mail: *anna.zamir.10@ucl.ac.uk*; *annazamir@gmail.com*

Objective: To demonstrate the feasibility of using X-ray phase-contrast tomography to assess internal organs in a post-mortem piglet model, as a possible non-invasive imaging autopsy technique.

Methods: Tomographic images of a new-born piglet were obtained using a free-space propagation X-ray phase-contrast imaging setup at a synchrotron (European Synchrotron Radiation Facility, Grenoble, France). A monochromatic X-ray beam (52 keV) was used in combination with a detector pixel size of $46 \times 46\,\mu m^2$. A phase-retrieval algorithm was applied to all projections, which were then reconstructed into tomograms using the filtered-back projection algorithm. Images were assessed for diagnostic quality.

Results: Images obtained with the free-space propagation setup presented high soft-tissue contrast and sufficient resolution for resolving organ structure. All of the main body organs (heart, lungs, kidneys, liver and intestines) were easily identified and adequately visualized. In addition, grey/white matter differentiation in the cerebellum while still contained within the skull was shown.

Conclusion: The feasibility of using X-ray phase-contrast tomography as a post-mortem imaging technique in an animal model has been demonstrated. Future studies will focus on translating this experiment to a laboratory-based setup.

Advances in knowledge: Appropriate image processing and analysis enable the simultaneous visualization of both soft- and hard-tissue structures in X-ray phase-contrast images of a complex, thick sample.

INTRODUCTION

Perinatal autopsy is important for future pregnancy management, medical research and mortality statistics.[1] However, perinatal autopsy rates continue to fall, for a variety of reasons, including parental reluctance on moral or religious grounds, fear of cosmetic effects and a lack of understanding of the potential benefits.[2] This has led to the development of less-invasive post-mortem imaging techniques, such as MRI, being developed both as adjuncts and alternatives for conventional autopsy.[3,4] While post-mortem MRI has been shown to have a high diagnostic accuracy for internal organ imaging, detailed imaging is time consuming, expensive and may not be available in all centres.[4]

Conventional X-ray CT is quicker, easier to use and more widely available; however, it suffers from poor soft-tissue differentiation, especially in foetuses and children, in the absence of exogenous contrast media.[5]

X-ray phase-contrast imaging (XPCi) methods have the potential to overcome some of these problems. Unlike in conventional X-ray imaging, in XPCi, image contrast is based on the phase shift induced by the object instead of its attenuation.[6] In general, the complex refractive index of a material is given by $n\,(E) = 1 - \delta\,(E) + i\,\beta\,(E)$, where E is the X-ray energy, δ is responsible for the phase shift and β describes the attenuation properties of the material. At diagnostically relevant X-ray energies, δ is considerably larger than β, by up to three orders of magnitude.[7] Hence, the sensitivity of XPCi systems to variations in δ typically results in higher image contrast, particularly for soft tissues with naturally weak attenuation.

In order to present a first proof-of-principle of the feasibility of using XPCi for post-mortem imaging, we performed an experiment which involved two simplifications. First, we used the simplest XPCi method—free-space propagation (FSP)—under ideal conditions, *i.e.* at a synchrotron. Secondly, rather than human tissue, we used a foetal piglet as an animal model owing to its anatomical similarity to a human foetus in shape, size and general anatomy.

Figure 1. Schematic representation of a free-space propagation setup. The X-ray beam is wide in the horizontal (x) direction and narrow in the vertical (y) direction. The large object-to-detector distance (z_{od}), jointly with the beam coherence, gives rise to the phase signal.
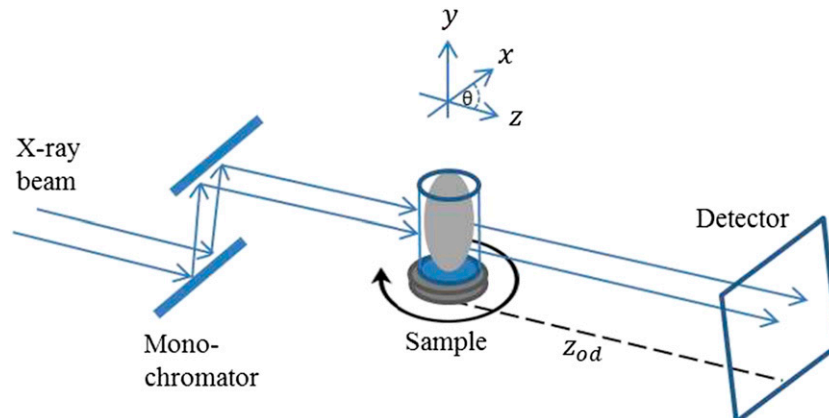
METHODS AND MATERIALS

Sample preparation

A deceased new-born piglet, acquired from a local farm near the imaging site which supplies the food industry, was used as a test sample. Ethical approval was not required, and no animals were sacrificed for the purpose of this experiment, since the animal died naturally at birth.

For ease of prolonged handling, and since it has been reported to have no effect on the resulting image contrast,[8] the piglet was fixed using a 4% formalin solution. It was then placed in a custom-made plexiglass cylinder (10-cm diameter, 25-cm height) which maintained it in a fixed (vertical, head up) position during the CT scan.

Free-space propagation experimental setup

In FSP, phase sensitivity is achieved by illuminating a sample with a spatially coherent X-ray beam and placing a high-resolution detector at a sufficient distance downstream of the sample. The presence of the sample in the beam's path causes both attenuation and phase shifts to the beam. Since the beam is spatially coherent, the induced phase shifts result in an interference pattern which can be detected as variations in the recorded intensity.[9] Different phase-retrieval methods can then be applied to the acquired image in order to obtain a phase image.[10] A schematic of the FSP setup is shown in Figure 1.

The experiment was conducted at the ID17 biomedical beamline of the European Synchrotron Radiation Facility (ESRF, Grenoble, France). The source size is approximately 132 μm (horizontal) × 24 μm (vertical) (full width at half maximum) and is located approximately 143 m from the end of the optics hutch where the sample was placed. A double-crystal Si (111) monochromator provided X-rays with an energy of 52 keV. The beam's vertical dimension was approximately 5 mm. The sample was placed downstream of the monochromator, on translation and rotation stages. The object-to-detector distance (Z_{od}) was approximately 10 m. Images were acquired using a FReLoN CCD (charge-coupled device) camera, custom-developed in-house at the ESRF (Grenoble, France), with an effective pixel size of $46 \times 46\ \mu m^2$. The recorded field of view was 2048 × 110 pixels, corresponding to approximately 5 mm vertically, and thus required vertical scanning of the sample to cover its full length (approximately 25 cm). This was achieved by acquiring a 5-mm-thick, full CT data set of the sample at a given vertical position, then shifting the sample vertically by slightly <5 mm (to create an "overlap" and avoid missing information) and repeating the procedure until the full volume was covered. As the sample was also larger than the horizontal field of view, projections were acquired using the half-acquisition method.[11] CT scans were acquired over 360° using 8000 projections and 15 ms exposure time per projection. For each scan, a total of 40 images without a sample (*i.e.* "flat fields") were taken: 20 images immediately before the scan and 20 images immediately after. These were averaged and used to correct the FSP projections for beam and detector non-uniformities.

Image processing

Each of the raw FSP projections was normalized by division by the flat-field image, and composite projections of the full sample were created to account for using the half-acquisition method. In order to extract the phase information, a phase-retrieval algorithm was applied to each projection. The algorithm[12] assumes *a priori* knowledge of the complex refractive index of different materials in the sample, which, for soft tissue and bone at 52 keV, were taken from the International Commission on Radiation Units and Measurements (ICRU) 44 database.[13] In general, the filter used in this phase-retrieval step creates artefacts at the edges of a projection. To avoid these, the top and bottom of projections from following sub-CT scans had to be overlapped and averaged before performing the phase retrieval. Therefore, minor intensity changes between consecutive CT scans caused inherent problems to the normalization process, only at the borders between separate scans. CT reconstruction was performed using the filtered-back projection algorithm, using the Ram–Lak filter. The Amira platform (Mercury Computer Systems, Germany) was used for three-dimensional (3D) volume visualization and manipulation. 3D volume rendering was performed to assist with organ identification, and slice orientation was varied to allow for best organ visualization, similar to the procedure in standard clinical practice.

Table 1. Contrast-to-noise ratio (CNR) values for different organs in raw and phase-retrieved free-space propagation (FSP) slices

Tissues compared	Raw FSP CNR	Phase-retrieved FSP CNR
Heart—artery	1.1	5.5
Kidney—intestine	1.6	7.1
Small intestine—free peritoneal fluid	1.0	4.6
Kidney—liver	1.6	5.9
Muscle—stomach	1.2	9.5

Image analysis

The entire data set was assessed by an experienced paediatric radiologist (OJA, with 8 years' experience in clinical imaging), to identify internal organs and other structures, assess tissue contrast and optimize 3D organ visualization, analogous to a clinical setting. Seven organ or body systems were assessed, including the heart, lungs, kidneys, liver, small and large bowels (intestines), brain and spinal cord, and bones (vertebrae), as these are typically the most important organs to assess in human post-mortem imaging.

Unfortunately, as we had no access to a standard CT scanner, the phase images shown have not been directly compared with conventional CT scans of the same sample. However, to provide quantitative evidence to support the findings of the radiologist, it is possible to exploit the fact that in a raw FSP slice, the area contrast (*i.e.* away from edges of a detail which will exhibit the typical phase-induced fringes) is caused merely by sample absorption. Therefore, the contrast-to-noise ratio (CNR) was assessed and compared in multiple organs for both raw FSP slices and phase-retrieved slices. The CNR was defined as the difference in mean values of two closely spaced tissues (each calculated from a homogenous area away from edges), divided by the standard deviation of the background noise (measured in the air gaps in the cylinder). More generally, it should also be noted that the superiority of phase-contrast images over absorption contrast images—mainly in terms of signal-to-noise ratio and CNR—has been previously reported in samples of similar size and complexity.[14]

RESULTS

Table 1 provides a quantitative comparison by reporting the measured CNR values for different organs for both raw and phase-retrieved FSP slices. In all cases, CNR values were higher in phase-retrieved slices, with an increase factor ranging from 3.7 to 7.9. This can be visually appreciated in Figure 2, which presents both a raw FSP (Figure 2a) and phase-retrieved slice (Figure 2b), each windowed to optimize the visualization of the same region in the heart. The heart's structure was clearly visible in the phase-retrieved slice, owing to the increased soft-tissue contrast arising from sensitivity to phase shifts induced by the sample.

All seven organ or body systems were visualized with sufficient contrast and adequate resolution, using the described FSP setup. Figure 3 displays images of key organs for the purpose of a post-mortem examination. The anatomy of the heart is depicted with a high level of detail (Figure 3a,b); all four cardiac chambers with the great vessels were identified, with high-quality imaging of the cardiac valves (such as the pulmonary valve, Figure 3b). The striations seen in Figure 3a are an artefact of the normalization process of subvolume CT scans, which were vertically joined to visualize the whole volume (see "Methods and materials"). Lung structure is also shown clearly (Figure 3c,d); the architecture shown in Figure 3d was visualized by magnifying and reconstructing the minimum intensity projection over 24 slices. The anatomy of the right kidney is shown in two orthogonal views (Figure 3e,f) and in a false-colour maximum intensity projection image obtained by using 31 slices (Figure 3g). The renal pelvis emerging into the

Figure 2. Phase-retrieval provides higher soft-tissue contrast (b) compared with a raw free-space propagation (a) image of the same axial slice through the thorax, showing normal heart and lungs. Large bilateral post-mortem pneumothoraces are demonstrated (non-pathological).
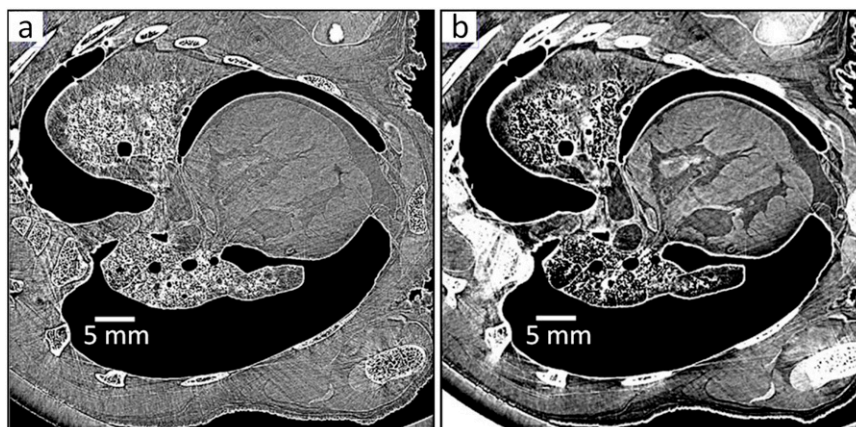
Figure 3. Excellent soft-tissue contrast allows for a high level of detail of the organs typically identified and examined at autopsy. Internal cardiac structures are clearly demonstrated, including ventricular chambers in sagittal (a) and oblique axial orientations (b) and the outflow tract valves [*e.g.* pulmonary valve; arrow in (b)]. Lung windowing permits detailed examination of the lung parenchyma (coronal; c) which may be further enhanced using magnified minimum intensity projection images for structural detail (d). Axial and coronal images of the kidney (e and f, respectively) allow the normal collecting system and ureter (e; arrow) to be identified, and the internal vascular anatomy can be assessed on false-coloured reconstructed maximum intensity projection images (g).
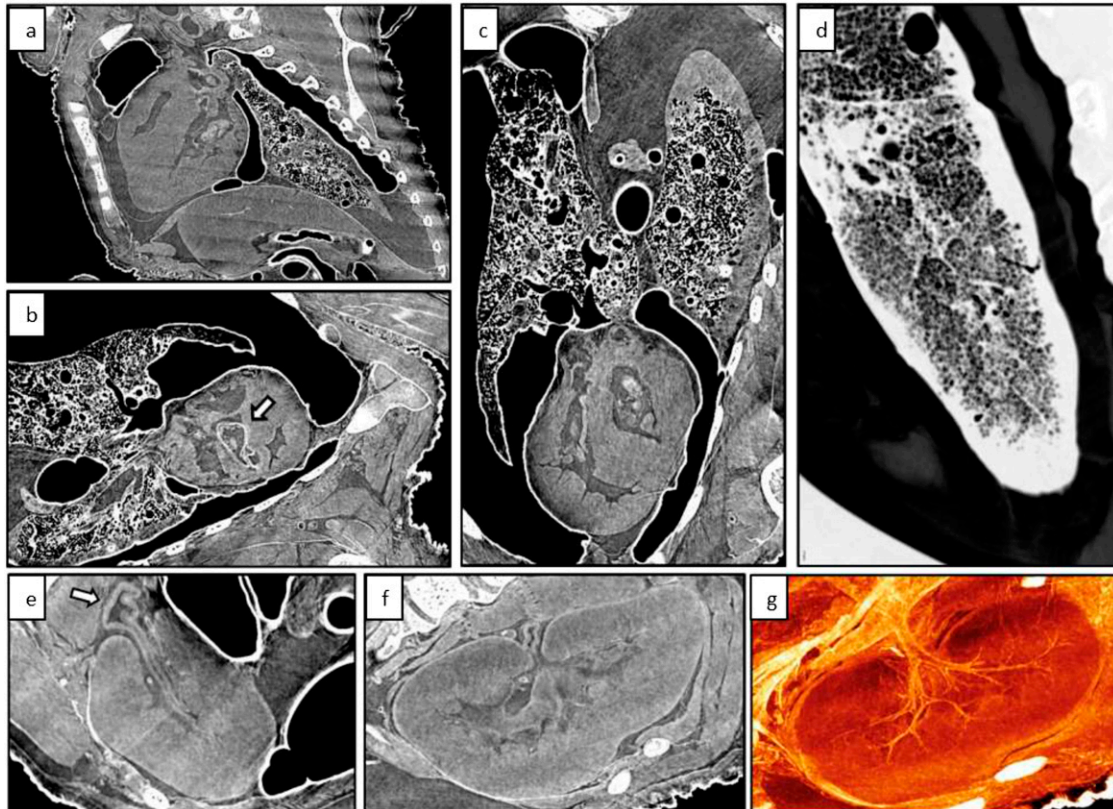
proximal ureter is clearly shown in Figure 3e, and the vascular system is depicted in detail using multiplanar reconstruction techniques in Figure 3g; no intravascular contrast agent was required.

A coronal slice of the head is shown in Figure 4a; the contrast was optimized for soft tissue, causing the nasal canals and skull to appear overexposed. The high soft-tissue contrast in the eyes and olfactory bulb can be easily appreciated. Figure 4b shows a magnified slice of the brain (maximum intensity projection using 28 slices), in which white and grey matter in the cerebellum can be clearly differentiated, despite very similar δ values and the comparably strong signal from the adjacent skull.

Figure 5 demonstrates the high dynamic range of this imaging technique. In this figure, good soft-tissue contrast is evident when visualizing the small intestine (Figure 5a), liver (Figure 5b) and eye, down to the cranial nerves (Figure 5c). However, although the protocol was designed to optimize visualization of soft tissue, this does not compromise the quality of bone imaging, as effective windowing allows the visualization of both soft- and hard-tissue details. Indeed, Figure 5d demonstrates the high resolution and contrast of a vertebral body obtained with the FSP setup. Therefore, XPCi allows all different components

of a complex biological sample to be adequately resolved through the acquisition of a single data set.

DISCUSSION AND CONCLUSION

The results shown in this study indicate that XPCi CT could be a useful tool for whole-body post-mortem imaging, as it can provide high-contrast, high-resolution images of a relatively large and complex biological sample.

This study was performed using an FSP setup with synchrotron radiation. While FSP does not require the use of any optical elements and is therefore easy to implement, it requires highly coherent radiation, which limits its use outside specialized facilities. Nevertheless, recent novel methods have emerged that enable its implementation with conventional X-ray sources, such as those typically used in a clinical setting, thus making it potentially more widely available. These are discussed in ref 6 and include grating-based approaches, FSP with microfocal sources and analyser crystal-based approaches. Our group focuses on the development of edge illumination (EI) XPCi CT with commercially available sources, which was recently demonstrated to provide similar image quality to XPCi at synchrotrons (Hagen C, et al, manuscript submitted; compare also the supplementary material in ref 15 with the quantitative analysis in ref 16).

Figure 4. Brain imaging. A coronal slice through the brain, showing normal globes and olfactory structures (a). A sagittal maximum intensity projection image of the cerebellum showing normal white/grey matter differentiation (b).
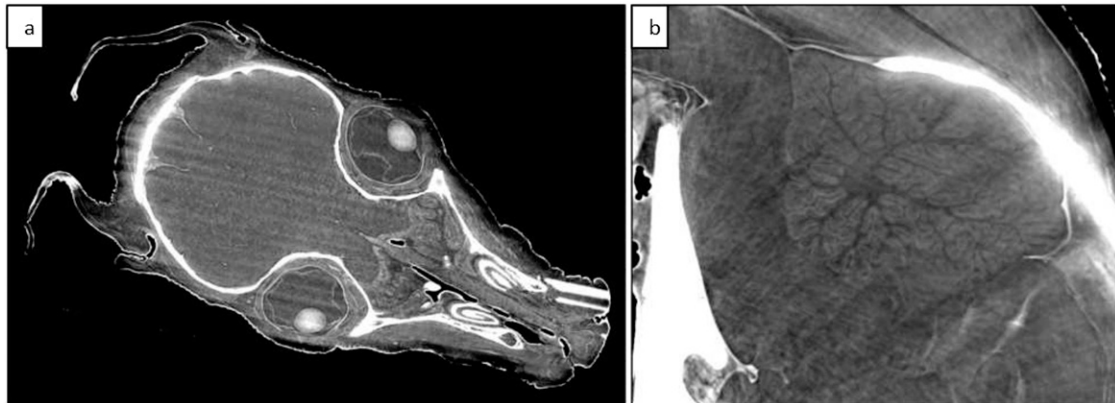

The possibility of translating these results by using EI or another lab-based XPCi method supports their relevance.

The results shown in table 1 provide some form of comparison between phase-contrast X-ray imaging and conventional absorption-based X-ray imaging; however, these are drawn from the same data set which was optimized for phase imaging. In future experiments, a direct comparison with conventional CT should be made. Where no access to a CT scanner exists, a comparison can be made with an additional data set obtained

Figure 5. High soft-tissue contrast allows detailed examination of normal structure. Examples include oblique axial slices of the abdomen demonstrating normal intestinal wall and lumen (a; arrow) and hepatic architecture (b; arrow). Magnified oblique sagittal views through the orbits and globe allow the optic nerve to be assessed (c; arrow). Using different windowing provides high bone detail, such as seen in this axial slice through a single vertebral body (d).
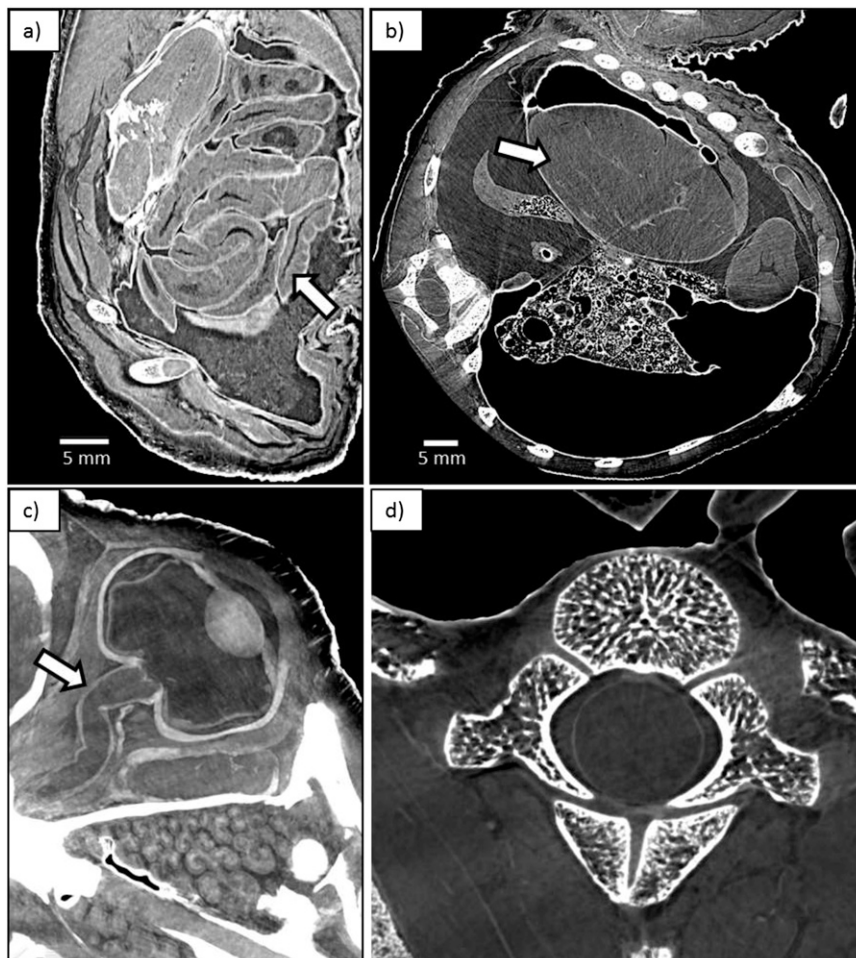
with a low propagation distance, such that it approximates to a conventional CT setup.

Although we used a foetal piglet in this study, the results are likely to be generalizable to other similar animal models and human foetal tissue. We specifically chose this animal model owing to the size and body component similarities to human tissue. All of the shown structures would be of potential significance during a conventional human perinatal autopsy. A variety of techniques are currently required for human post-mortem imaging in order to cover a range of body sizes, with different technical attributes for soft tissue and bone imaging. Were XPCi to be available and optimized for human use, particularly for smaller foetuses, then XPCi CT would have the potential to become a clinically useful post-mortem imaging modality, alongside other existing techniques including conventional CT and MRI.

In conclusion, the results of this study demonstrate that XPCi CT is possible in relatively large, unstained biological samples and that major organs can be visualized with the required contrast and resolution for the purpose of clinical diagnostic use. This experiment was conducted as a first proof-of-principle study using synchrotron radiation and an animal model and successfully demonstrates the feasibility of using XPCi methods for such applications. Future studies will focus on translating this application to a clinical laboratory: our group will pursue this by using the EI XPCi method, while other groups might propose alternative solutions, ultimately increasing the chances of achieving an effective translation. Successful development will allow XPCi CT to be introduced into clinical practice, initially to provide an alternative to standard perinatal autopsy, since the method will potentially be widely accessible, cheaper and able to achieve high throughput.

REFERENCES

1. Burton JL, Underwood J. Clinical, educational, and epidemiological value of autopsy. *Lancet* 2007; **369**: 1471–80. doi: 10.1016/S0140-6736(07)60376-6

2. McHaffie HE, Fowlie PW, Hume R, Laing IA, Lloyd DJ, Lyon AJ. Consent to autopsy for neonates. *Arch Dis Child Fetal Neonatal Edition* 2001; **85**: F4–7.

3. Thayyil S, Cleary JO, Sebire NJ, Scott RJ, Chong K, Gunny R, et al. *Post-mortem* examination of human fetuses: a comparison of whole-body high-field MRI at 9.4 T with conventional MRI and invasive autopsy. *Lancet* 2009; **374**: 467–75. doi: 10.1016/S0140-6736(09)60913-2

4. Thayyil S, Sebire NJ, Chitty LS, Wade A, Chong WK, Olsen O, et al. *Post-mortem* MRI *versus* conventional autopsy in fetuses and children: a prospective validation study. *Lancet* 2013; **382**: 223–33. doi: 10.1016/S0140-6736(13)60134-8

5. Arthurs OJ, Taylor AM, Sebire NJ. The less invasive perinatal autopsy: current status and future directions. *Fetal Matern Med Rev* 2013; **24**: 45–59. doi: 10.1017/S0965539513000065

6. Bravin A, Coan P, Suortti P. X-ray phase-contrast imaging: from pre-clinical applications towards clinics. *Phys Med Biol* 2013; **58**: R1–R35. doi: 10.1088/0031-9155/58/1/R1

7. Lewis RA, Hall CJ, Hufton AP, Evans S, Menk RH, Arfelli F, et al. X-ray refraction effects: application to the imaging of biological tissues. *Br J Radiol* 2003; **76**: 301–8. doi: 10.1259/bjr/32889803

8. Mollenhauer J, Aurich ME, Zhong Z, Muehleman C, Cole AA, Hasnah M, et al. Diffraction-enhanced X-ray imaging of articular cartilage. *Osteoarthr Cartilage* 2002; **10**: 163–71. doi: 10.1053/joca.2001.0496

9. Cloetens P, Barrett R, Baruchel J, Guigay JP, Schlenker M. Phase objects in synchrotron radiation hard X-ray imaging. *J Phys D Appl Phys* 1996; **29**: 133–46. doi: 10.1088/0022-3727/29/1/023

10. Langer M, Cloetens P, Guigay JP, Peyrin F. Quantitative comparison of direct phase retrieval algorithms in in-line phase tomography. *Med Phys* 2008; **35**: 4556–66. doi: 10.1118/1.2975224

11. Sztrókay A, Diemoz PC, Schlossbauer T, Brun E, Bamberg F, Mayr D, et al. High-resolution breast tomography at high energy: a feasibility study of phase contrast imaging on a whole breast. *Phys Med Biol* 2012; **57**: 2931–42. doi: 10.1088/0031-9155/57/10/2931

12. Beltran MA, Paganin DM, Siu KK, Fouras A, Hooper SB, Reser DH, et al. Interface-specific X-ray phase retrieval tomography of complex biological organs. *Phys Med Biol* 2011; **56**: 7353–69. doi: 10.1088/0031-9155/56/23/002

13. ICRU (International Commission on Radiation Units and Measurements). *Tissue substitutes in radiation dosimetry and measurement, ICRU Report 44*; 1989.

14. Horng A, Brun E, Mittone A, Gasilov S, Weber L, Geith T, et al. Cartilage and soft tissue imaging using X-rays: propagation-based phase-contrast computed tomography of the human knee in comparison with clinical imaging techniques and histology. *Invest Radiol* 2014; **49**: 627–34. doi: 10.1097/RLI.0000000000000063

15. Hagen CK, Munro PR, Endrizzi M, Diemoz PC, Olivo A. Low-dose phase contrast tomography with conventional X-ray sources. *Med Phys* 2014; **41**: 0707011. doi: 10.1118/1.4884297

16. Hagen CK, Diemoz PC, Endrizzi M, Rigon L, Dreossi D, Arfelli F, et al. Theory and preliminary experimental verification of quantitative edge illumination X-ray phase contrast tomography. *Opt Express* 2014; **22**: 7989–8000. doi: 10.1364/OE.22.007989